# 18

# Bacterial Cellulose-Based Biomimetic Composites

Thi Thi Nge[1,2], Junji Sugiyama[2] and Vincent Bulone[3]
[1]*Present Address: Biomass Technology Research Centre, National Institute of Advanced Industrial Science and Technology, 3-11-32, Kagamiyama, Higashi-Hiroshima, Hiroshima 739-0046;*
[2]*Research Institute for Sustainable Humanosphere, Kyoto University, Uji, Kyoto 611-0011;*
[3]*School of Biotechnology, Royal Institute of Technology, SE-10691 Stockholm*
[1,2]*Japan*
[3]*Sweden*

## 1. Introduction

As the primary component of plant cell walls, cellulose is a major constituent of plant biomass and represents the most abundant biopolymer on earth. It is also a representative of microbial extracellular polymers synthesized by some bacteria. The cellulose synthesized by the *Gram-negative* bacterium *Gluconacetobacter xylinus* (previously named *Acetobacter xylinum*) has been extensively studied since the pioneering work of Hestrin and Schramm (1954). A single *G. xylinus* cell may polymerize up to 200,000 glucose molecules as a linear β-1-4 glucan chain that are excreted extracellularly as subelementary fibrils. The latter are assembled into microfibrils that aggregate to form ribbons with a hierarchical structure (Hestrin & Schramm, 1954). The matrix of interwoven ribbons constructs a pellicle which has a dense surface side and a gelatinous layer on the opposite side that remains in contact with the liquid medium (Klemm et al., 2001; Nge & Sugiyama, 2007).

Typically, networks of well-separated nano- and microfibrils of bacterial cellulose create extensive surface area and hold a large proportion of water while maintaining a high degree of structural coherence. The water content of never-dried bacterial cellulose pellicles is about 99% (w/w). A high density of inter- and intra-fibrillar hydrogen bonds offers a great deal of mechanical strength. The elastic modulus of dried bacterial cellulose is known to be around 15-30 GPa. Besides being chemically identical to plant cellulose, bacterial cellulose is produced in a virtually pure form free from hemicelluloses, pectins and lignin, which are present in plant cellulosic matrices. Moreover, the in vivo biocompatibility evaluation of bacterial cellulose in rats has demonstrated that it is well integrated into the host tissues and does not elicit any chronic inflammatory reaction, making it a potentially interesting scaffolding material for tissue engineering (Helenius et al., 2006). The unique physical and mechanical properties of bacterial cellulose as well as its purity can be exploited for multiple applications that range from high quality audio membranes, electronic paper, and fuel cell to biomedical materials (Klemm et al., 2001; Czaja et al., 2006).

In the biomedical area, bacterial cellulose can be used for wound healing applications (Czaja et al., 2006), micro vessel endoprothesis (Klemm et al., 2001), scaffolds for tissue engineered cartilage (Svensson et al., 2005) and tissue engineered blood vessels (Bäckdahl et al., 2006). Some of the materials based on bacterial cellulose, such as new skin substitutes and wound dressing materials, are now commercially available (Czaja et al., 2006). Other biomedical applications such as the use of bacterial cellulose as a regenerative aid to correct skeletal defects are under investigation.

Aging is accompanied by the progressive deterioration of the skeletal system, such as in osteoporosis, and by increasing dental problems. There is an increasing demand to design and fabricate high-performance biocompatible materials that mimic the unique quality of natural bones. Bone tissues composite materials composed of specialized cells, an organic matrix rich in collagen fibers and an inorganic mineral phase consisting essentially of calcium and phosphate. The organic fraction synthesized by osteoblasts mediates the formation of apatite (calcium-phosphate minerals) crystals into distinct microstructures that accommodate the mechanical forces encountered in bone tissues (Gilmcher, 1998).

Since the mineral phase of bone is mainly composed of apatite, cements based on synthetic hydroxyapatite (HA; $Ca_{10}(PO_4)_6(OH)_2$) and other calcium phosphate salts are among the most investigated materials for dental and orthopaedic applications in reconstructive surgery. Because of their biocompatibility, moldability, bone bonding ability, osteoconductivity, non-toxic and noninflammatory effects (de Groot, 1983), these bioceramics are widely employed as bone substitute materials. For instance outstanding results were reported for the treatment of periodontal osseous defects and alveolar ridge augmentation (Murugan & Ramakrishna, 2004). However, these materials have some disadvantages, such as brittleness, rapid resorption, migration of cement particles from the implant site and considerably inferior mechanical strength compared to natural bone, which limit their application as load bearing structures at the site of skeletal defects.

Fabrication of matrix-assisted bioceramic composites by in situ precipitation or bone-like apatite coating of biocompatible and/or biodegradable polymers by biomimetic approaches has become an attractive alternative method to improve the mechanical stability and strength of the desired implant. The polymer matrices also serve as binders to prevent migration of the cement particles, in addition to enhance mechanical integrity owing to their toughness and flexibility. Biomimetic approaches involve soaking polymer matrices in a simulated body fluid (SBF) whose ion concentration is equal to that of human blood plasma at physiological pH and temperature. Alternatively, the polymer matrices are soaked at 37˚C in calcium and phosphate solutions prepared with a Ca/P ratio of 1.67, similar to the Ca/P ratio of synthetic HA. The concept of apatite formation includes (i) the heterogeneous nucleation of apatite crystals in the presence of surface functional groups of polymer matrices and (ii) the increased supersaturation of the surrounding fluid to accelerate the nucleation process and growth. Several studies have reported the use of various kinds of organic polymers, e.g. silk fibre (Takeuchi et al., 2003), gelatin (Bigi et al., 2002), phosphorylated chitin fibres (Yokogawa et al., 1997) and polylactic acid (Maeda et al., 2002).

In the present study, the biocompatible polymer bacterial cellulose (BC) with its ultra-fine network nature, abundant surface hydroxyl groups and natural mechanical properties is used to investigate the possibility of fabricating BC-based materials that mimic the properties of collagen fibrils in bone. It is widely accepted that surface chemical structures exert a significant influence on the formation of apatite layers on materials surfaces in

physiological conditions. They promote cells attachment, proliferation, growth and differentiation when the materials are exposed to biological environments. Surface modification of BC and engineering of the culture medium of *G. xylinus* were performed to render the BC materials biomimetic. Surface modification was performed by TEMPO (2,2,6,6—tetramethylpyperidine-1-oxyl)-mediated oxidation to introduce carboxyl functional groups, which are known to be effective inducers of apatite nucleation. TEMPO, a water-soluble and stable nitroxyl radical, is well-known for its catalytic and selective oxidation of primary hydroxyl groups of polysaccharides under aqueous conditions (Saito & Isoagi, 2004; Saito & Isogai, 2005; Montanari et al., 2005). Culture medium modification was performed by the addition of an amino sugar (*N*-acetylglucosamine) in the culture medium normally used for BC production. This amino sugar moiety is the monomer unit of chitin, the second most abundant natural biopolymer, which is commonly found in shells of marine crustaceans and cell walls of fungi (Roberts, 1992). It also shares the structural feature of glycosaminoglycan (GAGs) which are unbranched heteropolysaccharides consisting of the repeating unit [uronic acid-amino sugar]. GAGs are extracellular matrix (ECM) constituents of skeletal tissues, in addition to collagen fibrils and apatite minerals. GAGs are considered to play an important role in stimulating chondrogenesis by modulating chondrocyte morphology, differentiation, and function (Suh & Matthew, 2000; Di Martino et al., 2005).

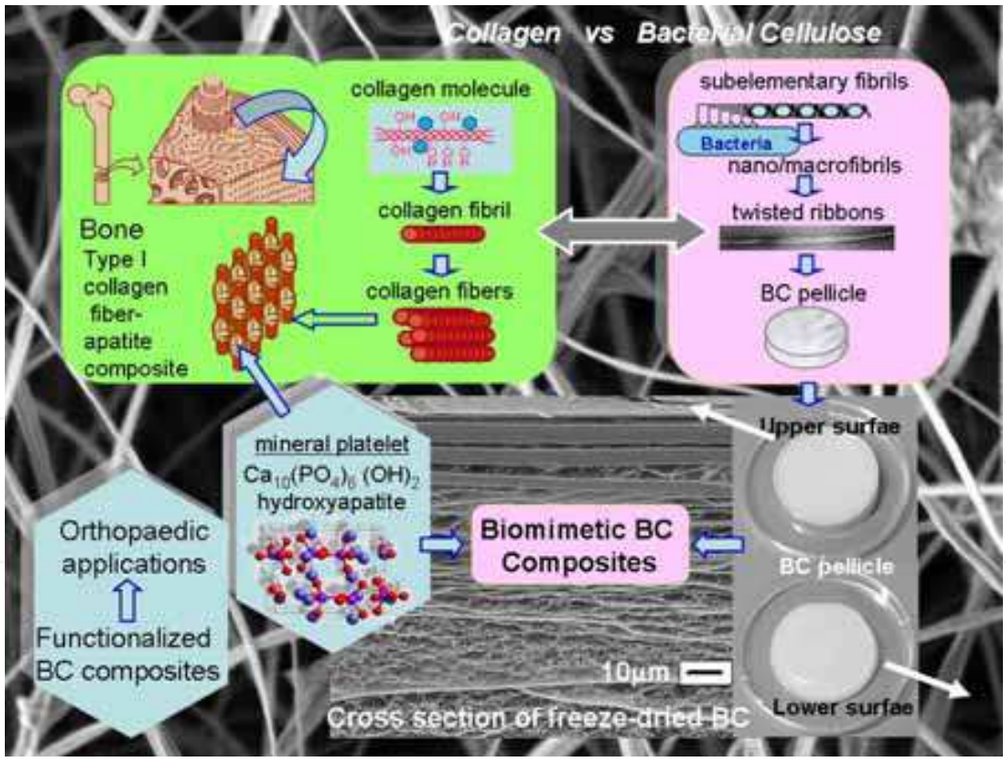


Fig. 1. Schematic representation of bacterial cellulose-based biomimetic composites with potential osteological applications

Considering the function of GAGs in ECM of skeletal tissues, our strategy was to attempt incorporating an amino sugar in bacterial cellulose to prepare a biomimetic ECM. The overall

objective is to fabricate a new generation of BC-based biomimetic composites with potential osteological applications and to study the morphological and structural properties of the modified BC. The workflow comprises the following three main parts (see also Figure 1):

1. production of bacterial cellulose from standard culture medium as well as modified culture medium (addition of *N*-acetylglucosamine), and surface modification by TEMPO-mediated oxidation;
2. apatite formation by soaking the surface modified bacterial cellulose in a simulated body fluid;
3. apatite formation by alternatively soaking the surface modified bacterial cellulose and the bacterial cellulose containing *N*-acetylglucosamine in calcium and phosphate solutions.

## 2. Preparation of bacterial cellulose

### 2.1 Microbial synthesis of bacterial cellulose

The bacterial strain *Acetobater aceti* (AJ12368), a cellulose producing species closely related to *G. xylinus*, and the Schramm-Hestrin (SH) medium (Hestrin & Schramm, 1954) were used for bacterial cellulose (BC) production. The culture medium consists of 2% glucose, 0.5% peptone, 0.5% yeast extract, 0.27% sodium hydrogen phosphate ($Na_2HPO_4$) and 0.115% citric acid monohydrate. The pH of the medium was adjusted to 5 with 1N HCl and autoclaved at 120˚C for 20 min. The cells used as the inoculum were statically pre-cultured in test tubes at 27˚C for two weeks. The thick gelatinous membrane (BC pellicle) was squeezed aseptically to remove cells embedded inside the pellicle. A 25 mL cell suspension (~1.3× $10^7$ cells/mL) was then transferred to 500 mL fresh medium and successively distributed (9 mL/well) into 6-well culture plates (Iwaki-Asahi Techno Glass, Japan). The BC pellicles (~35 mm Φ) recovered after static culture at 27˚C for 9 days were purified in two steps. First, the pellicles were placed in boiling distilled water for 1h, followed by an incubation in 0.1 M NaOH at 80˚C for 2h. The pellicles were then washed with distilled water until neutral pH was reached. Some of the purified pellicles were used for TEMPO-oxidation and some were subjected to freeze-drying after having been flash-frozen in liquid nitrogen. Hereafter, the freeze-dried BC is designated as "native" BC.

#### 2.1.2 Surface modified bacterial cellulose (BC-TEMPO and BC-TEMPO-Ca)

Surface modification of the never-dried BC was performed by TEMPO-mediated oxidation to introduce carboxyl functional groups at C(6) primary hydroxyl groups of the cellulose chains (Nge & Sugiyama, 2007). The never-dried BC pellicles (dry weight of 0.15 ± 0.003 g) were suspended in distilled water (80 mL) containing TEMPO (0.0075 g) and sodium bromide (0.075 g) under continuous stirring. An appropriate amount of sodium hypochlorite solution corresponding to 2.42 mmole/g cellulose was added slowly. The reaction was carried out for 2h at pH 10.5 and 20˚C by addition of 0.5 M NaOH. The oxidation was quenched by adding 2 mL ethanol followed by the addition of 0.1 N HCl to reach neutral pH. Subsequently, the oxidized pellicles were washed with distilled water several times to remove residual reagents and subjected to freeze-drying as mentioned above. Hereafter, the freeze-dried TEMPO-oxidized bacterial cellulose pellicles are designated as BC-TEMPO. The carboxylate content of BC-TEMPO measured by conductimetric titration (Nge & Sugiyama, 2007) was 0.25 mmol/g cellulose. The oxidation conditions used for BC-TEMPO in this study were not the most optimal to limit the level of oxidation.

Some of the TEMPO-oxidized pellicles recovered after washing with distilled water were immersed in 0.1M $CaCl_2$ with stirring at room temperature for 6 h to exchange the sodium counterion of the carboxylate groups to calcium. The ion-exchanged TEMPO-oxidized BC pellicles were subjected to freeze-drying after washing with distilled water several times. Hereafter, these bacterial cellulose pellicles are designated as BC-TEMPO-Ca. The amount of calcium ions in BC-TEMPO-Ca measured by X-ray fluorescence analysis (MESA-500, Horiba Co., Japan) was 0.22 mmol/g cellulose. With a carboxylate content of 0.25 mmol/g cellulose and an ion exchange ratio of approximately 1:1, the formation of BC-$COOCa^+$ was predominant over $(BC\text{-}COO)_2Ca$ (Saito & Isogai, 2005).

### 2.2 Bacterial cellulose prepared from modified culture medium (BC-GlcNAc)

The amino sugar *N*-acetylglucosamine (GlcNAc) was added in the culture medium as a source of sugar together with the glucose normally used for BC production. The objective was to determine the optimal medium composition that allows the incorporation of a maximum number of GlcNAc residues in BC. The different compositions tested are presented in Table 1 and Figure 2.

| | Medium ID | Glucose (mg/100mL) | GlcNAc (mg/100 mL) |
|---|---|---|---|
| SH medium | 2000 | 20 | 0 |
| Modified SH medium | 1604 | 16 | 4 |
| Modified SH medium | 1010 | 10 | 10 |
| Modified SH medium | 0416 | 4 | 16 |
| Modified SH medium | 0020 | 0 | 20 |

* A medium ID was given for the different sugar compositions. The BC produced from the different media are named after the corresponding medium ID

Table 1. Composition of glucose and *N*-acetylglucosamine at a fixed carbon source of 2%

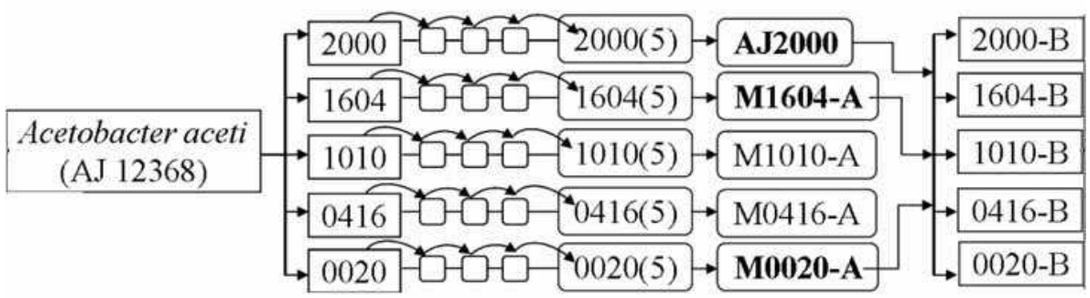


M: modified medium containing GlcNAc (starter culture obtained by repeated transfer (5 times) of inoculum at 3 days of growth)
A: GlcNAc-containing medium/GlcNAc-containing BC (inoculation using the same sugar contents as for the starter culture)
B: GlcNAc-containing BC with different sugar content (inoculation from AJ 2000, M1604 A, and M0020A as starter cultures)

Fig. 2. Experimental setup for *N*-acetylglucosamine (GlcNAc) incorporation in BC; the first 2 digits represent the glucose concentration and the later 2 represent the GlcNAc concentration (mg/100mL).

As shown in Figure 2, adaptation of *Acetobacter* cells to the presence of the amino sugar was performed by 5 repeated transfers of 3-day-old inoculum into the medium containing different GlcNAc concentrations. The inoculum culture time of 3 days was selected based on cell density estimated by measuring the optical density at 600 nm. The volume ratio of inoculum to medium was 1:10 for all compositions. The microbial production of cellulose was performed by static culture fermentation as described in section 2.1.1.

The effect of sugar composition on the rate of cellulose production was studied. The cellulose dried mass produced in the medium devoid of GlcNAc (AJ2000) increased over 14 days and reached 6.41 mg/mL, with an exponential mass production between days 3 to 7 followed by a slower production rate until day 14 (Figure 3a). In the presence of GlcNAc, the lag phase was shorter than with the AJ2000 medium as judged by a higher mass production at days 3 and 4. This lag phase was followed by an increasing mass phase until day 7 and levelling-off. However, the masses produced over 14 days in the media containing the sugars mixtures were lower than in the absence of GlcNAc, with 4.74, 3.33, and 1.29 mg cellulose/mL for M1604-1604A, M1604-1010B and M1604-0416B, respectively. The cellulose production in the medium containing GlcNAc only (M1604-0020B) was low (0.19 mg/ mL) throughout the culture period, most likely reflecting a low cell growth. At a fixed total carbon source of 2%, the decrease in cellulose mass with increasing GlcNAc concentrations reflects the limitation of cellulose formation although GlcNAc enhances the initial production rate. There was a greater consumption of glucose rather than GlcNAc by the cells. The mass therefore decreased with decreasing glucose concentrations at a fixed total carbon source. Shirai et al. also reported the accumulation of GlcNAc during incubation in mixed sugars media. For their analyses, the authors determined the time course of sugar consumption by using Schales' modified procedure for total sugar and a glucose oxidase/peroxidase system for glucose (Shirai, et al., 1994).

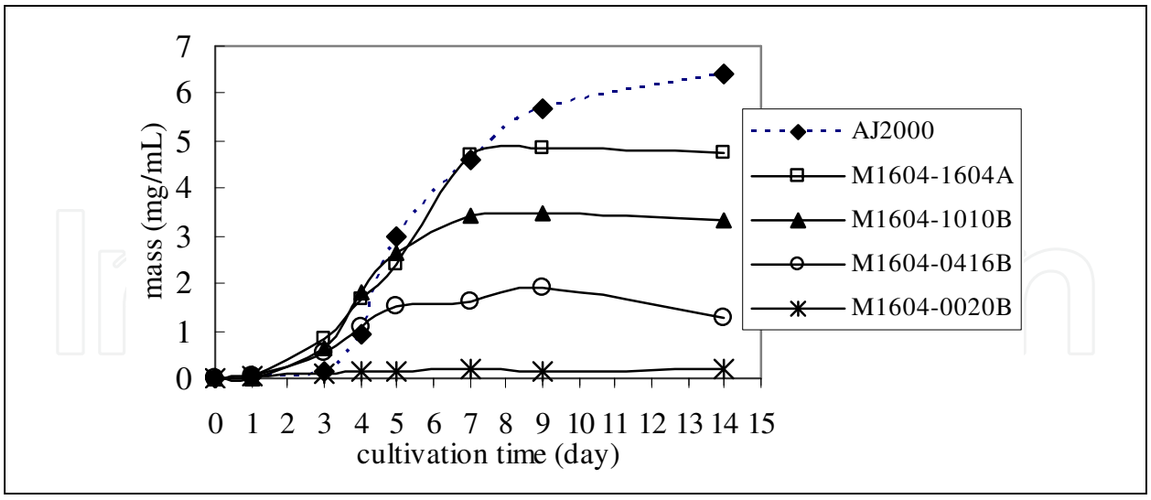


Fig. 3a. Cellulose production in the presence of glucose, mixed sugars, or GlcNAc as a function of cultivation time

The pH (Figure 3b) of the mixed sugar medium decreased rapidly from its initial value of 5.0 to the lowest value of 3.53-3.98 within 4 days, whereas a gradual decrease in pH was observed in the medium containing glucose only (AJ2000), with the lowest pH of 3.5 at day 7. The phases were followed by an increase of the pH value of from 4.9 to 5.3 in the media

AJ2000 to M1604-0416B (Figure 3b). The decrease in pH was due to the conversion of glucose to keto/gluconic acids by a membrane-bound *Acetobacter* dehydrogenase (Klemm et al., 2001). Klemm et al. reported that the gluconic and 5-keto gluconic acids were detected from the second day and third day of cultivation in the culture broth of *G. xylinus* AX 5 by means of HPLC. The acid may affect cellulose production by first lowering the environmental pH and then possibly the intracellular pH, resulting in the stabilization and/or activation of key enzyme(s) for cellulose biosynthesis. On the other hand, a sharp decrease in pH may limit not only cellulose formation, but also lower the medium pH to suboptimal levels for cell viability and cellulose synthesis. The highest mass gain obtained until day 7 (Figure 3a) during the gradual decrease of pH in AJ2000 is consistent with the above assumption. The pH of the medium containing GlcNAc only (M1604-0020B) showed a different trend: the pH remained nearly constant after it had dropped to 3.98 (Figure 3b).

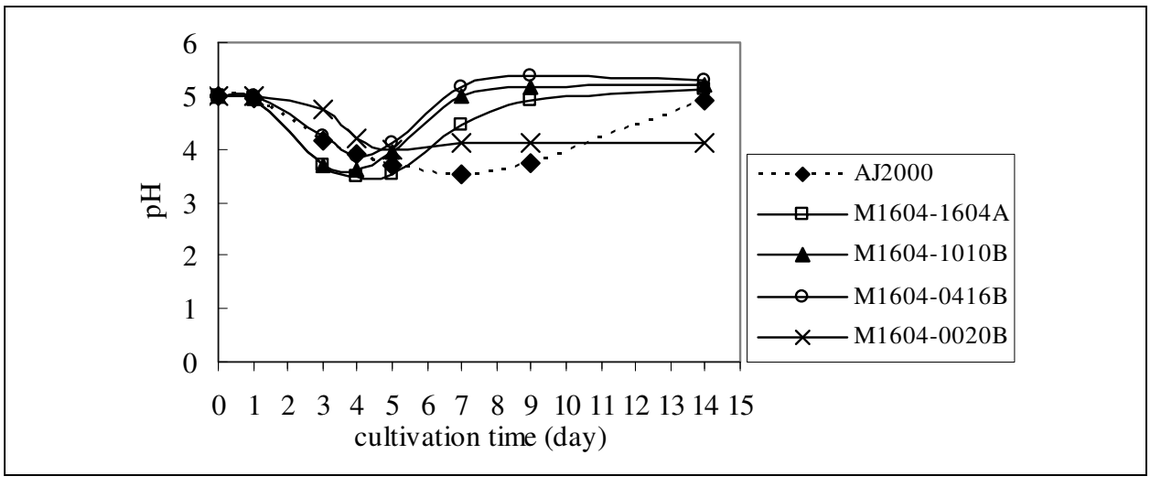


Fig. 3b. pH of the media containing glucose, mixed sugars, or GlcNAc only as a function of cultivation time

Based on the results shown in Figure 3, the cultivation time in further experiments was fixed to 7-9 days for the media containing GlcNAc. Figure 4 shows the effect of the type of starter culture on cellulose dry mass as a function of GlcNAc content in the medium.

In general, the mass decreased with increasing GlcNAc concentrations in all 3 types of starter cultures. Cellulose produced in AJ2000 and M1604A showed the similar trend, whereas a slightly lower mass profile was observed for cellulose produced in M0020A. Hence, cell adaptation was not critical in starter cultures containing small amounts of GlcNAc (M1604A).

### 2.2.1 Determination of GlcNAc incorporation using a radiolabelling method

A previous study has reported the determination of GlcNAc incorporated in bacterial cellulose by using GC-MS (Lee et al., 2001). Here, the amount of incorporated GlcNAc was examined by a labelling method based on the use of radioactive GlcNAc (1.85 MBq *N*-acetyl-D-[1-$^{14}$C] glucosamine; Moravek Biochemicals, Inc., California, U.S.A.) and Liquid Scintillation Counting (LSC, Packard Tricarb, Perkim Elmer Inc.). Small-scale labelling was carried out in 1 mL culture media containing different amounts of non-radioactive GlcNAc and inoculated using starter cultures in AJ2000, M1604A, M1010A, M0416A, and M0020A.

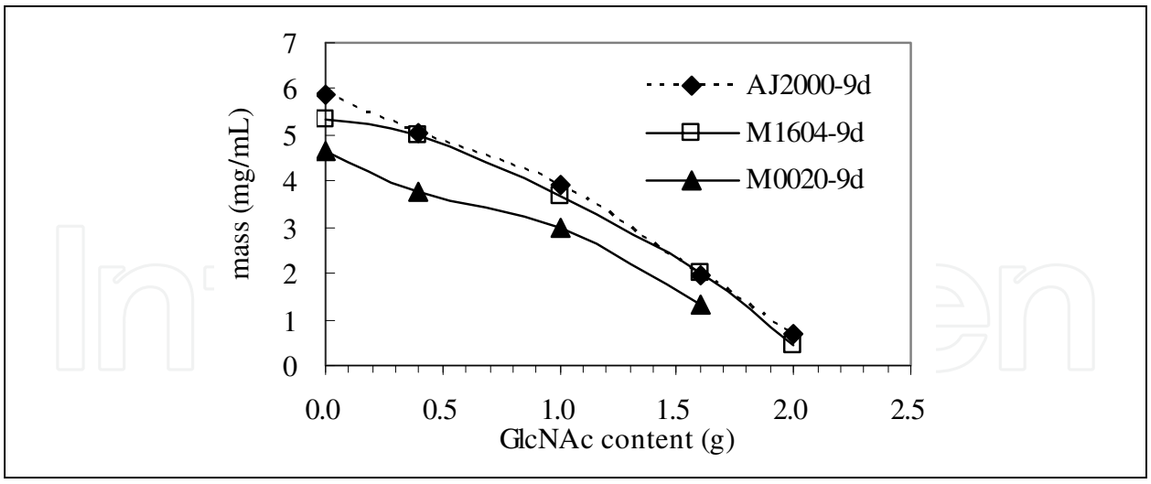


Fig. 4. Cellulose production from different starter cultures as a function of GlcNAc content in the culture medium

The molar concentration of the added radioactive GlcNAc was negligible compared to the concentration of non-radioactive sugar in the culture medium. The static cultures were incubated for 7 days in the same conditions as for bulk production (see section 2.2). The small pellicle formed was taken out at days 2, 3, 5, and 7 followed by purification (washing with distilled water, boiling with 0.1 M NaOH at 80°C for 90 min, and washing with distilled water until neutral pH was reached). After addition of scintillation cocktail (Ultima Gold, Packard) in the vials containing the purified BC pellicles, the radioactivity corresponding to the incorporated GlcNAc was measured by liquid scintillation. The total amount of incorporated GlcNAc was then calculated from the levels of radioactivity measured. Parallel runs were also performed in the absence of radioactive GlcNAc to determine the cellulose dry mass.

The mole% of incorporated GlcNAc as a function of cultivation time from different starter cultures is shown in Figure 5a. A detectable level of GlcNAc incorporated was observed at day 2. The radioactivity measured increased until day 3 in M0416-0416A, M0020-0416B and M0020-1010B; and day 5 in M1010-1010A, M1604-1604A, M0020-1604B, and AJ2000-1604B. They were fairly stable after 5 days. It was concluded that the incorporation of GlcNAc occurred essentially in early incubation times, within 5 days. This finding was in agreement with the higher cellulose mass observed in the media containing mixed sugars compared to the medium containing glucose only (Figure 3a). The level of GlcNAc incorporated after 7 days was in the range 0.6-0.36 mole%, depending on the amount of non-radioactive GlcNAc present in the culture medium and the type of starter culture used.

Generally, the incorporation of GlcNAc decreased with increasing GlcNAc concentrations (decreasing glucose content) in the culture medium. The presence of high GlcNAc concentrations with concomitant decrease in glucose content may limit the activity of cellulose biosynthesis (Figure 3a) since a negligible cellulose mass was produced in the medium containing GlcNAc only. The time course of cellulose production in the medium containing a high concentration of non-radioactive GlcNAc (Glucose : GlcNAc - 0416) showed a similar trend regardless of the type of starter culture used. The effect of the type of starter culture was observed in the glucose:GlcNAc - 1010 and 1604 media. The starter cultures containing the same sugar content (e.g. inoculation of M1604 with an inoculum

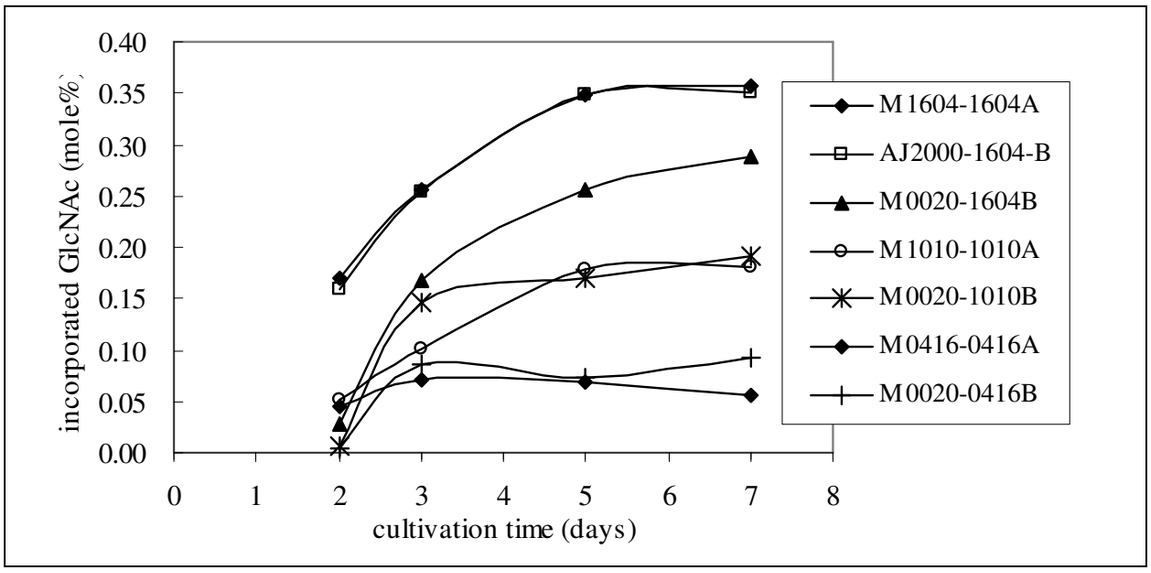


Fig. 5a. Amount of incorporated GlcNAc in bacterial cellulose as a function of cultivation time

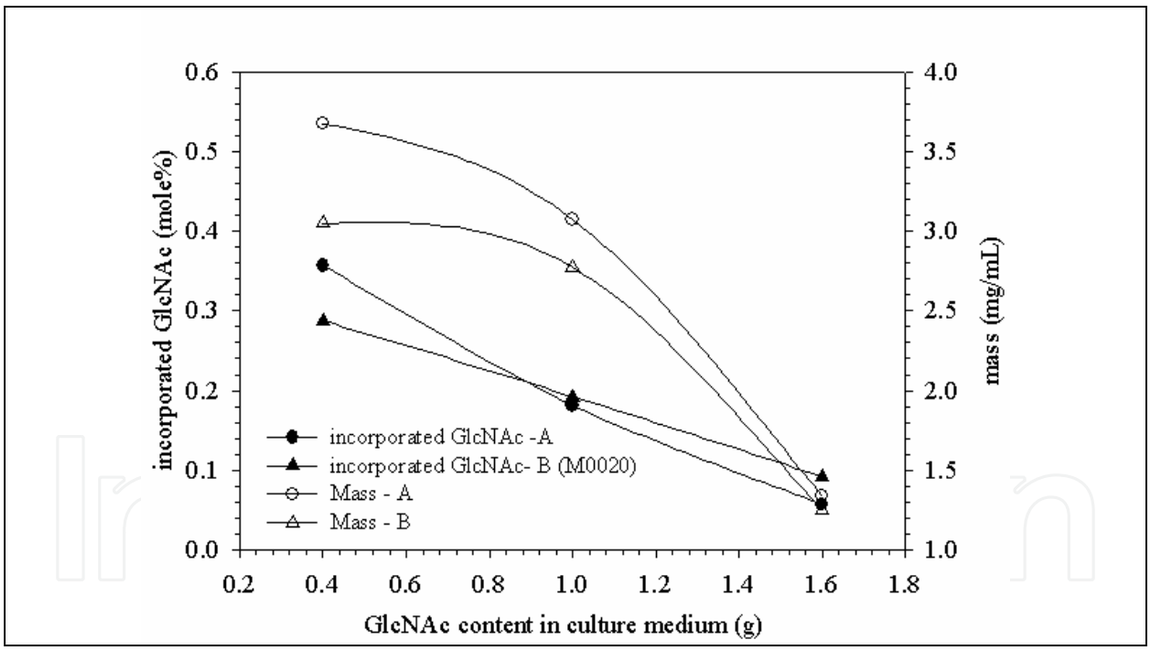


Fig. 5b. Cellulose dry mass and amount of incorporated GlcNAc as a function of non-radioactive GlcNAc content in culture medium (A denotes M1604-1604A, M1010-1010A, and M0416-0416A; B denotes M0020-1604B, M0020-1010B, and M0020-0416B).

prepared in the 1604 medium) led to higher amounts of GlcNAc incorporation than inoculums from the medium containing GlcNAc only (i.e. inoculation of the 1604 medium with a M0020 inoculum). This effect was more significant for the 1604 medium than for the 1010 medium, where a higher incorporation rate was observed throughout the cultivation time. Moreover, the M1604-1604A cultures showed a similar trend as sample AJ 2000-1604B

(direct inoculation from a starter culture containing glucose only). This observation confirmed that no adaptation period in the presence of GlcNAc was necessary to obtain an increased GlcNAc incorporation into cellulose. The 1604 medium is the best suited for high GlcNAc cellulose incorporation and cellulose production under the conditions studied (Figure 5b) although the maximum incorporation obtained (0.36 mole%) is lower compared to other earlier studies (Shirai et.al, 1994; Lee et. al., 2001) which were based on the use of different *Acetobacter* strains and methods.

As only small amounts of GlcNAc can be incorporated during BC biosynthesis, we switched our strategy to the use of chitosan (deacetylated form of chitin) instead of GlcNAc and fabricated bacterial cellulose/chitosan porous scaffolds by freeze-drying TEMPO-oxidized BC microfibrils in suspension in a chitosan solution (Nge et al., 2010). By using this approach, one can control the ratio of BC and chitosan to obtain the desired properties.

### 2.2.2 Analysis of the morphology of BC-GlcNAc by electron microscopy

Microscopic observations of the synthesized BC-GlcNAc composite was performed by transmission electron microscopy (TEM; JEOL JEM 2000-EXII microscope) and field emission scanning electron microscopy (FE-SEM; JEOL JSM-6700F microscope).

In order to observe the nascent BC microfibrils after ribbon assembly and before the formation of interwoven network mats, on-grid sample preparation was carried out. Drops (10 µl) of cultivation medium inoculated with different starter cultures were placed on carbon-coated copper grids (200-mesh) and incubated at 27 ˚C for 2 days followed by a gentle washing with distilled water. Negative staining was performed with 2% uranyl acetate. The TEM micrographs of nascent BC microfibrils synthesized in media containing different concentrations of GlcNAc or glucose only are shown in Figure 6.

The network assembly had already formed in M1604-1604A, whereas ribbons were observed in AJ2000 and M1010-1010A. The formation of the network in M1604-1604A even at a 10-µl medium scale was an indication of the faster production rate during early incubation times, in agreement with the mass production profile shown in Figure 3a. A small increase in the lateral dimension of fibril aggregates (~80 - 125 nm) was observed in M1010 compared to AJ2000 (~60 - 105 nm), as judged from the flatten parts of the ribbons. Individual finer cellulose fibrils with lateral dimensions of 18-23 nm (arrow in Figure 6b) were observed in the M1604 medium. Because of network assembly in M1604, the lateral dimensions of the fibril aggregates were found to be in a wider range comprising 18-23 nm, 46-60 nm, 70-90 nm, and ~110 nm bundles.

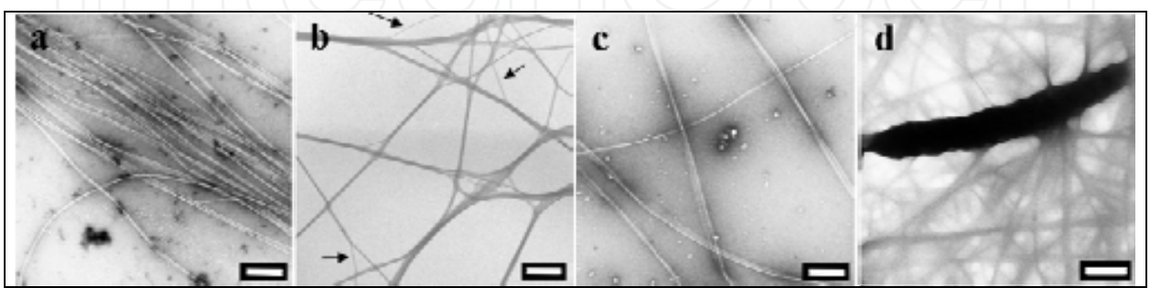


Fig. 6. TEM micrographs of bacterial cellulose ribbons from 2-day cultures of (a) AJ2000, (b) M1604-1604A, (c) M1010-1010A, and (d) an *Acetobacter* cell immobilized within a fibril network (7 day culture of M1010), scale bars = 500 nm

The presence of water soluble polysaccharides in the culture medium can affect the structure and formation of BC (Uhlin et al., 1995). The polymers can interfere with the assembly of microfibrils and bundles during extrusion of cellulose as elementary fibrils. In general, the sorption of these polysaccharides results in less ordered BC, as demonstrated by electron microscopy, X-ray diffraction, FT-IR, and solid-state NMR spectroscopy. Addition of the water soluble amino sugar GlcNAc in the culture medium in our study not only limits the cell activity but also affects the lateral dimensions of fibril aggregates to some extent. The reason of the latter effect is not clear. Either the interaction occurs after the glucan chain has been extruded in the extracellular medium or GlcNAc is first taken up in the intracellular compartment and incorporated in the glucan chains before their extrusion. According to the assumption of Ogawa and Tokura (1992), an acetamido-group-transferring enzyme is present in the bacterium and the UPD-GlcNAc synthesized in the cytoplasm as a precursor of peptidoglycan or lipopolysaccharides becomes a substrate of cellulose synthase.

The BC-GlcNAc pellicles obtained in a 6-well culture plate after 9 days of culture are shown in Figure 7. Because oxygen is required for the aerobic growth of *Acetobacter* cells and for cellulose production, the formation of cellulose occurs only at the upper film/air interface (aerobic zone). It is therefore assumed that the cellulose produced is gradually pushed down, while the new cellulose layers are constantly being built on the top of the mature cellulose (Scharamm & Hestrin, 1954). A surface layer built at the interface between the culture medium and air shows a dense pellicle surface (Figure 8a), especially in AJ2000. Because of the immobilization of the bacteria between the newly formed layer of cellulose fibril network and the gradually sinking older layers during cellulose production, the zone comprising the viable cells that are able to produce cellulose is also gradually drawn into the anaerobic part of the pellicle. The bacteria present in deeper zones are inactive for cellulose production. Therefore, the lower layer that remains in contact with the liquid medium is gelatinous and consists of a loose network. The middle compartment is a stack of several layers and the network density is intermediate to that of the upper and lower surface layers.

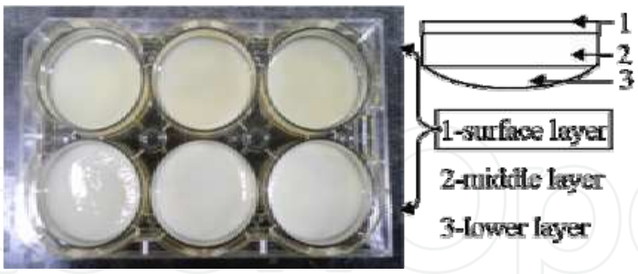


Fig. 7. Typical appearance of bacterial cellulose pellicles after 9 days of culture and schematic drawing of a pellicle layer

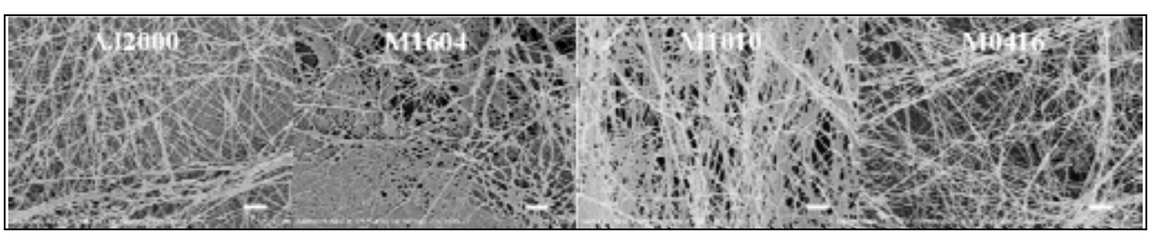


Fig. 8a. FE-SEM images of the surface layer of BC-GlcNAc; scale bar – 1 μm

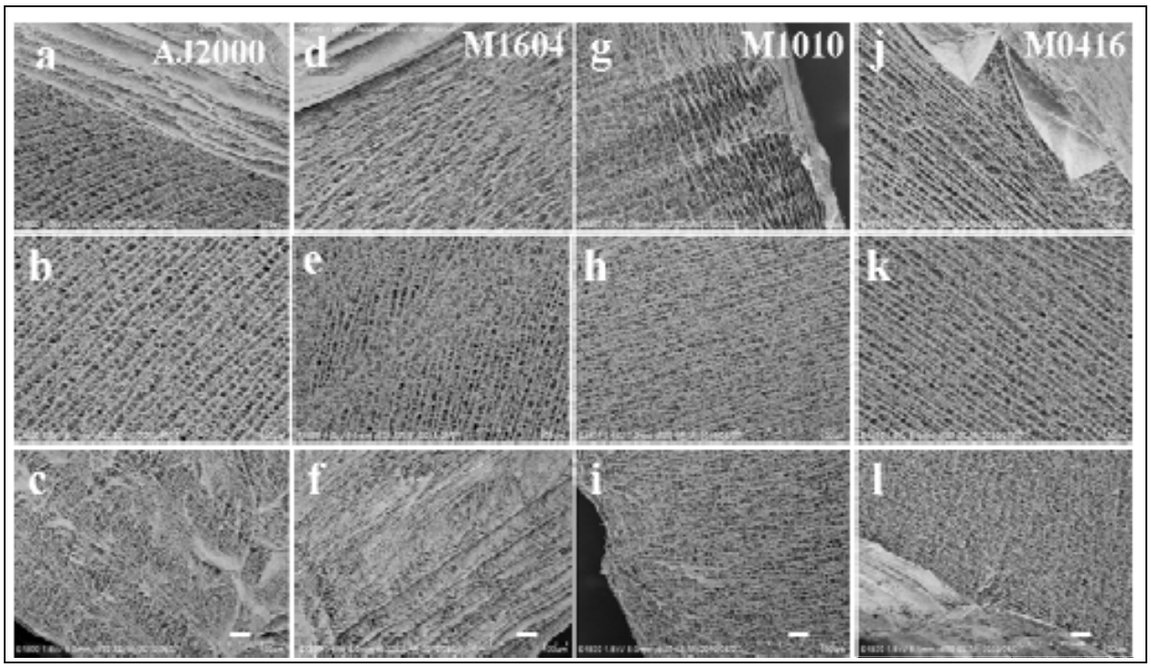


Fig. 8b. FE-SEM images of cross sectional surfaces of freeze-dried BC-GlcNAc pellicles; the first row (a,d,g,j) represents the upper part (pellicle-air interface during cultivation), the second row (b,e,h,k) the middle part, and the third row (c,f,i,l) the lower part (pellicle-culture medium interface) of the pellicles; scale bar – 20 µm

The ultrafine network structure of BC can be seen by FE-SEM in Figure 8b, which presents the cross sectional surface of the freeze-dried BC-GlcNAc pellicles. The physical three-dimensional microfibril network exhibits a hierarchical structure (Figure 8b).

The dense surface layer normally formed in native BC was not seen in M1010 and M0416. A thin surface layer is present instead, while the M1604 layer is similar to that of native BC (AJ2000). The network architecture of the frontier area between the surface layer and middle compartment is also varying between samples obtained from media containing different GlcNAc concentrations. An array of specific network patterns was observed in M1010 and M0416 compared with M1604. The texture of the middle compartment reflects the highly swollen network nature of the BC pellicle in its cultivation state. The never-dried BC pellicle is known to contain ca. 99% of water. This high water holding ability or high hydrophilicity is explained by the presence of pores forming ultrafine network structures, in addition to the occurrence of abundant hydroxyl groups in the cellulose molecular structure. The pore network structure was retained by during freeze-drying. The hollow space or pore size as well as the stacking lamellar pattern are different from each other. Judging from the FE-SEM images, the decreasing order of pore size is AJ2000 ≥ M0416 > M1604 > M1010, with sizes of 4-8 µm, 4-7 µm, 3-7 µm, 2-5 µm, respectively. The thickness of the lower layer also varied from sample to sample, with a few layers of fibril mat in AJ2000 and M1604 and only a thin layer in M1010 and M0416.

Variations in the formation of the dense surface layer and the loose lower layer as well as variations of their thickness reflects the activity of viable cells, which in turn reflects the dry mass of the BC pellicles produced from the respective culture media.

## 3. Formation of apatite on bacterial cellulose using a biomimetic approach

### 3.1 Soaking in a simulated body fluid (SBF)

In their study of bioactive glass-ceramic, Kokubo et al. (1990) developed a simulated body fluid (SBF), in which ion concentrations were nearly equal to those of human blood plasma at physiological pH and temperature.

| Order | Reagent | Amount | |
|---|---|---|---|
| | | SBF | 1.5 SBF |
| | | 1000 mL | 1000 mL |
| 0 | ultra-pure water | 750 mL | 750 mL |
| 1 | NaCl | 7.996 g | 11.994 g |
| 2 | $NaHCO_3$ | 0.350 g | 0.525 g |
| 3 | KCl | 0.224 g | 0.336 g |
| 4 | $K_2HPO_4.3H_2O$ | 0.228 g | 0.342 g |
| 5 | $MgCl_2.6H_2O$ | 0.305 g | 0.458 g |
| 6 | 1 M HCl | 40 mL | 60 mL |
| 7 | $CaCl_2$ | 0.278 g | 0.417 g |
| 8 | $Na_2SO_4$ | 0.071 g | 0.107 g |
| 9 | $(CH_2OH)_3CNH_2$ | 6.057 g | 9.086 g |
| 10 | 1 MHCl | Appropriate amount for adjusting pH | |

Table 2. Reagents and corresponding concentrations used for the preparation of SBF and 1.5 SBF (Kokubo et. al., 1990)

In our study, an SBF containing 1.5 time the ion concentrations of SBF (Table 2; 1.5 SBF) was prepared by dissolving sequentially reagent grade sodium chloride (NaCl), sodium hydrogen carbonate ($NaHCO_3$), potassium chloride (KCl), dipotassium hydrogen phosphate ($K_2HPO_4.3H_2O$), magnesium chloride hexahydrate ($MgCl_2.6H_2O$), calcium chloride ($CaCl_2$), and sodium sulphate ($Na_2SO_4$) (Wako Pure Chemical Ltd, Osaka Japan) in distilled water. The pH was adjusted to pH 7.4 ± 0.01 with tris-hydroxymethyl aminomethane ($NH_2C(CH_2OH)_3$) and 1 M HCl while maintaining the solution temperature at 36.5˚C. The stock solution was filtered through a 0.2 µm cellulose acetate filter and stored at 4˚C until used.
Freeze-dried BC samples, namely native-BC, BC-TEMPO, and BC-TEMPO-Ca, with a size of 10×10×5 mm and known weight were soaked in 10 mL of 1.5 SBF for three weeks at 37˚C. The SBF solution was renewed every 7 days. Samples were taken out at 2, 7, 14, and 21 days, washed thoroughly with distilled water and freeze-dried. The freeze-dried samples were weighed to determine the extent of mineral deposition. Four to five pieces were used for each BC sample for each designated soaking time.

### 3.2 Soaking in calcium and phosphate solutions

For alternate soaking processes, 0.05 M $CaCl_2$ (dissolving $CaCl_2$ in 50 mM Tris-HCl buffer at pH 7.4) and 0.03 M $NaH_2PO_4$ were prepared to obtain a Ca/P ratio of 1.67. Samples of native-BC, BC-TEMPO, BC-TEMPO-Ca and BC-GlcNAc of the same size as above were alternatively soaked in the calcium and phosphate solutions at 37˚C for 30 min with reciprocal shaking (50 strokes/min). The samples were rinsed thoroughly with distilled water between each soaking cycle. A total of 5 soaking cycles were performed. Samples were recovered at each soaking cycle and washed thoroughly with distilled water prior to freeze-drying and weighing.

## 4. Morphological and structural analyses

A field emission scanning electron microscope (FE-SEM, S 4100B, Hitachi Co., Japan and FE-SEM, JEOL, JSM-6700F, Japan) operating at an accelerating voltage of 1.5 kV was used to observe the ultrafine BC networks and the deposited minerals on the BC nano/microfibril surfaces. The BC samples were sputter coated with Pt-Pd and Pt for the FE-SEM-Hitachi and FE-SEM-JEOL microscopes, respectively. Formation of the calcium phosphate phases was determined by Fourier transformed infrared spectroscopy (Spectrum 2000 FT-IR, PerkinElmer) equipped with an attenuated total reflection (ATR) accessory and a single reflection diamond crystal ATR top-plate. The calcium phosphate (Ca/P) ratio of the deposited apatite was measured by inductively coupled plasma atomic emission spectroscopy (ICP-AES, Model SPS7800, Seiko Instrument, Japan). A known amount of apatite-deposited BC samples were soaked in 2% $HNO_3$ for 1 day to dissolve the calcium-phosphate mineral, followed by filtration through a 0.2 μm cellulose acetate filter and dilution to a concentration of about 5 ppm (detectable range of ICP-AES). The determination of the Ca/P ratios of all samples was based on calibration using synthetic hydroxyapatite (Wako Pure Chemical Ltd., Japan) as a standard.

### 4.1 BC samples soaked in a simulated body fluid (SBF)

Native-BC, BC-TEMPO and BC-TEMPO-Ca samples were used to investigate the effect of surface functional groups on apatite formation by soaking in 1.5 SBF. The SEM images of the apatite-deposited BC surfaces after 21 days of soaking in 1.5 SBF are shown in Figure 9. Calcium-phosphate minerals appear as hemispherical globules on the BC microfibril surfaces. These morphologies are similar to those reported in other studies using other substrates than BC. It can be seen that the globule sizes are clearly different between native-BC and BC-TEMPO-Ca (about 3 μm and <1 μm, respectively). The variation in size of the apatite globules under the same soaking condition reveals the importance of the microfibril surface structure in the nucleation process of apatite at initial soaking time (Sato et al., 2001; Uchida et al., 2003).

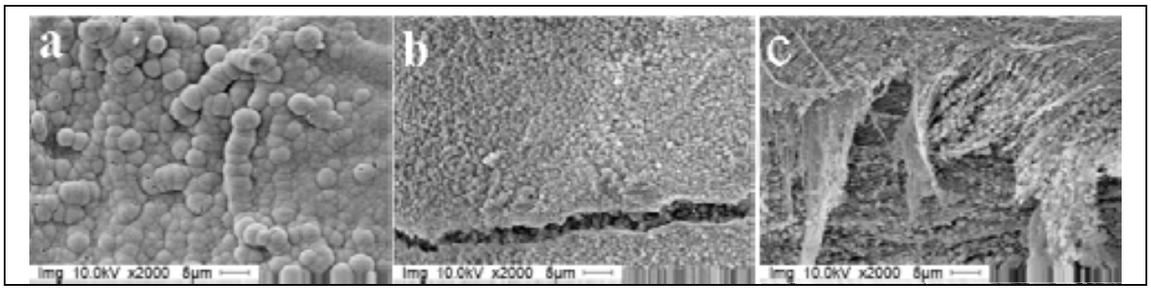


Fig. 9. SEM images of apatite-deposited BC surfaces: (a) Native-BC, (b and c) BC-TEMPO-Ca after 21 days of soaking in 1.5 SBF

The globule size in the BC-TEMPO sample is about 1.5 μm. The small apatite globules firmly adhere on the microfibril surface and form a uniform calcium-phosphate layer (compare Figures 9b and c). The presence of carboxylate groups on the BC microfibril surface (BC-TEMPO) and further ion-exchange treatment with calcium (BC-TEMPO-Ca) significantly affects the rate of apatite nucleation. A large number of nuclei grew competitively on BC-TEMPO-Ca leading to a smaller average size than for the BC-TEMPO and native-BC

samples. In other words, multiplication of mineralization or formation of more crystals may occur in BC-TEMPO-Ca, whereas a progressive mineralization by increase in size of the crystals or crystal growth may occur in native-BC, as in bone matrix mineralization and calcification of enamel, respectively (Rey et al., 1991a).

It was found that the apatite globules were composed of a cluster of thin-filmed flakes, which can be seen by TEM (Figure 10a). The specimen was prepared by a slight scratching of the BC-TEMPO surface with a razor blade and dispersion in 10% ethanol. A drop of the sample suspension was loaded on a 200-mesh carbon-coated copper grid. Microdiffraction was performed using a low dose electron probe on a ~100 nm diameter area, with a camera length of 15 cm and 2.8 s exposure. The micrograph and diffraction diagram were recorded on MEM films (Nge & Sugiyama, 2007). Depending on the particular orientation, the crystals exhibit an electron-dense needle-like appearance. The electron diffraction pattern (Figure 10b) taken from crystal clusters on microfibril surfaces indicates the (002) and (211) planes of the apatite crystal (Kim et al, 1996) together with the (004), (200), and (110) planes of cellulose microfibrils (Koyama et al., 1997).

By examining the weight gain at each soaking time interval, it was found that the relative amount of calcium-phosphate phase deposited on the BC microfibril surfaces increased with the soaking time, with a continuous consumption of Ca and P ions from the surrounding fluid. The BC-TEMPO-Ca samples, which exhibited the smallest apatite globules, showed the highest deposit weight, whereas the larger globule size in Native-BC was characterized by the lowest deposited weight after 21 days. The Ca/P molar ratio analysed by ICP-AES was 1.52 ± 0.09, 1.50 ± 0.08, and 1.45 ± 0.04 for Native-BC, BC-TEMPO, and BC-TEMPO-Ca, respectively, after 21 days soaking in 1.5 SBF, while it was of only 1.37 ± 0.08, 1.39 ± 0.02 and 1.31 ± 0.05 for a soaking time of 2 days (Nge & Sugiyama, 2007). Although the Ca/P ratio increased with the soaking time, the values for all the BC samples are lower than the theoretical value of 1.67 for hydroxyapatite ($Ca_{10}(PO_4)_6(OH)_2$).

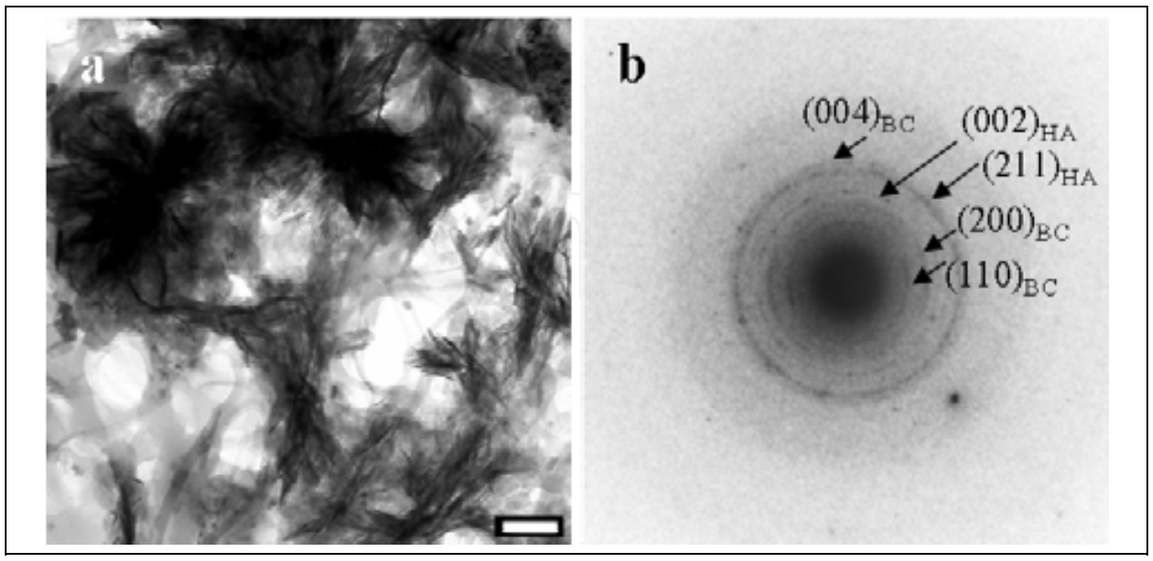


Fig. 10. (a) TEM micrograph of a cluster of apatite crystals deposited on a BC-TEMPO microfibril surface during 21 days of soaking in 1.5 SBF, and (b) Electron diffraction pattern of a cluster of individual crystals from a. scale bar – 500 nm

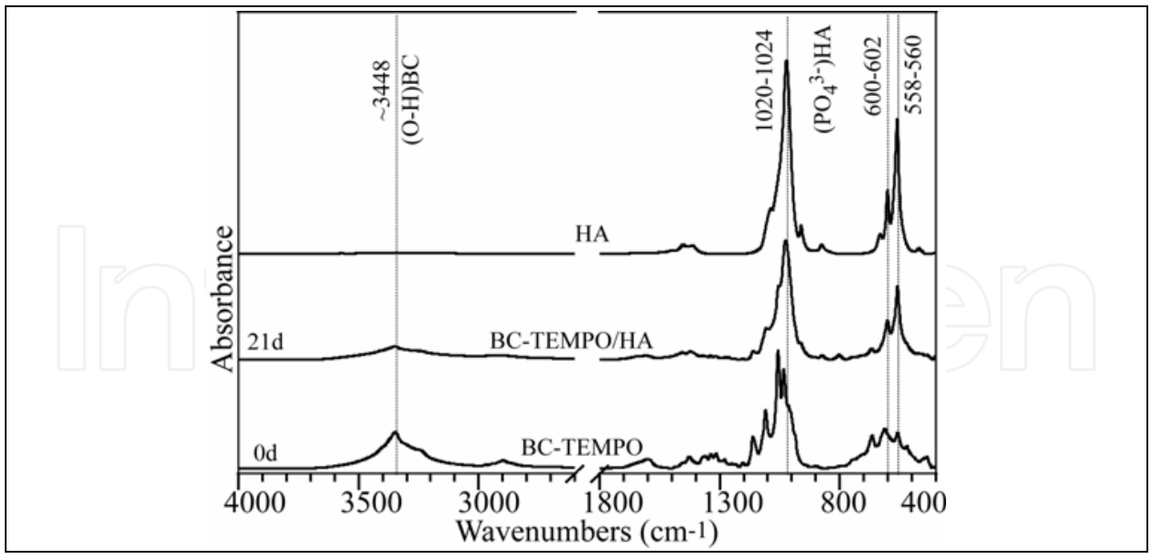


Fig. 11. Typical FT-IR spectra of BC-TEMPO, synthetic hydroxyapatite (HA) and apatite-deposited BC-TEMPO (BC-TEMPO/HA) after 21 days of soaking in 1.5 SBF

The calcium-phosphate phases thus formed are calcium deficient compared to hydroxyapatite. The lower Ca/P ratio was due to the substitution of the trivalent $PO_4^{3-}$ ions by divalent ions such as acid phosphate groups ($HPO_4^{2-}$) and carbonate groups ($CO_3^{2-}$). As a result, vacancies at $Ca^{2+}$ cationic sites in the apatite structure occurred during the formation of the calcium-phosphate phase (Elliott et al., 1985; Ray et al., 1989). The detailed information relative to the calcium-phosphate phases obtained with soaking times of 2 d, 7 d, 14 d, and 21 d was revealed by the ATR-FTIR spectral features, as described in our recent paper (Nge & Sugiyama, 2007). The FTIR spectral feature corresponding to the 2-21 days of soaking time indicated that the crystalline phase nucleated on the BC microfibril surfaces was calcium-deficient carbonated apatite resulting from the initial formation of octacalcium phosphate (OCP) or OCP-like calcium phosphate phases. The formation of calcium-deficient carbonated apatite can be explained by the presence of a $PO_4^{3-}$ absorption peak at 1020-1024 $cm^{-1}$ as shown in Figure 11. This peak arises from crystalline imperfections of nonstoichiometric apatite containing $HPO_4^{2-}$ and/or $CO_3^{2-}$ groups (Rey et al.1991b). The stoichiometric hydroxyapatite usually displays this characteristic peak at ~1030 $cm^{-1}$. In addition, the peaks at 600-602 $cm^{-1}$ and 558-560 $cm^{-1}$ observed in the BC-TEMPO/HA samples are also characteristic of the phosphate absorption band.

### 4.2 BC samples soaked in calcium and phosphate solutions

Native-BC, BC-TEMPO, BC-TEMPO-Ca, and BC-GlcNAc samples were used in alternate soaking processes. The biomimetic deposition of a calcium-phosphate coating on several BC samples was performed by alternative soaking of 1 $cm^2$ freeze-dried BC samples in 0.05 M $CaCl_2$ and 0.03 M $Na_2HPO_4$ at 37 ˚C, with 50 strokes/min and 30 min/cycle. A total of 5 cycles were performed for all BC samples. The weight-gain of calcium-phosphate deposited on the BC samples at each soaking cycle, the Ca/P ratio and morphology of the Ca-P crystals were determined.

The alternate soaking method showed a similar result as described in section 4.1., where the newly formed calcium-phosphate globules varied in size between the different BC samples.

FE-SEM images of apatite-deposited BC surfaces after 5 soaking cycles are shown in Figure 12. The size of the newly formed apatite globules on native-BC (4-6 μm) was much larger than for BC-TEMPO (1.5- 2 μm). In both cases, the globules were larger than those formed in 1.5 SBF, with respectively ~ 3 μm and ~1.5 μm for the native-BC and BC-TEMPO soaked in 1.5 SBF. The globules on BC-TEMPO-Ca, however, have a similar size with both soaking methods. The larger sizes formed using the alternate soaking method may be due to a relatively higher ion concentration in the calcium and phosphate soaking solutions than in 1.5 SBF, as well as to a more rapid soaking cycle (30 min interval as opposed to 21 days for the 1.5 SBF soaking method). As the lower layer of the BC pellicle (Figure 7) consists in general of a looser network than the surface layer, the apatite crystals formed on the microfibril surfaces in the lower layer exhibit a slightly different morphology. The apatite globules in the BC-TEMPO sample exhibit a more defined shape with a honeycomb-like three-dimensional structure composed of thin plate-like crystals (Figure 12e). Instead, thin plate-like crystals spread upward in all direction in the BC-TEMPO-Ca samples (Figure 12f). It is noteworthy that the surface functional groups or surface structure plays an important role in the initial step of apatite nucleation and governs the following mineralization process by either multiplication or progressive mineralization.

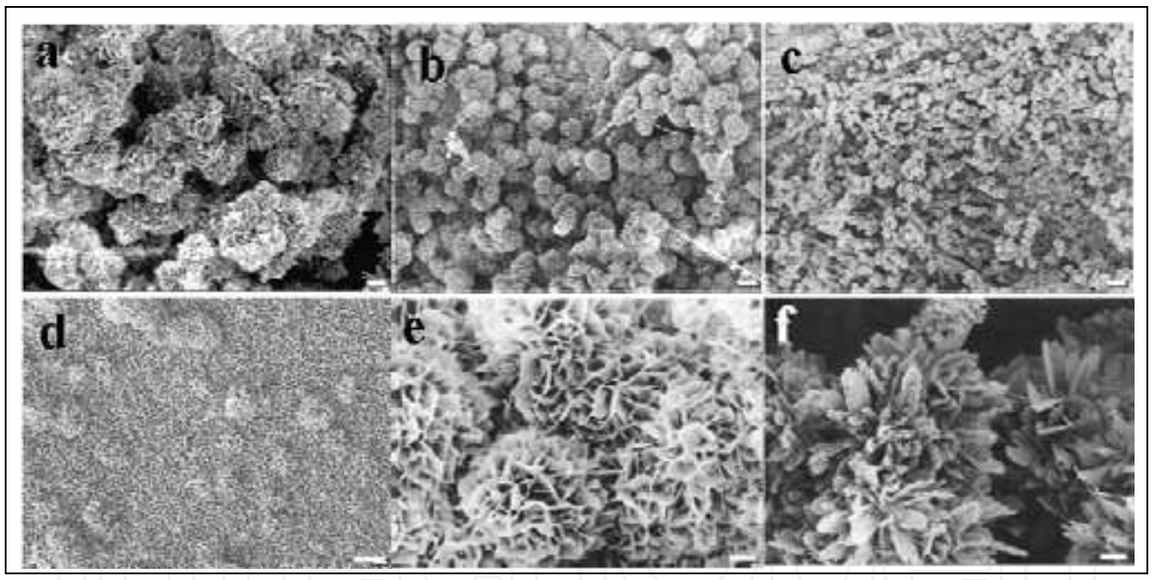


Fig. 12. FE-SEM images of apatite-deposited BC surfaces after 5 cycles of alternate soaking in calcium and phosphate solutions. (a) Native-BC, (b) BC-TEMPO, (c) BC-TEMPO-Ca, (d) BC-GlcNAc (M1604-1604A), (e) magnified view of apatite globules formed on the lower surface of the BC-TEMPO sample and (f) on the lower surface of the BC-TEMPO-Ca sample. Scale bars, 2 μm for a-d, 500 nm for e and f.

The apatite-deposited BC-GlcNAc (M1604-1604A) surface in Figure 12d, however, showed a different morphology compared with native-BC and BC-TEMPO. The crystal growth seemed to spread along the surface, with the initial formation of a monolayer followed by the formation of apatite globules of about 1-1.5 μm on the existing monolayer. The effect of the proportion of incorporated GlcNAc and type of starter culture used for the inoculation on apatite formation was also observed by FE-SEM (Figure 13).

In general, the Ca-P mineralization may take place by spreading as a monolayer along the BC surface layer, followed by further crystal growth upon the existing layer. Sample M1604-1604A, which exhibited the highest GlcNAc incorporation among all BC-GlcNAc samples, showed a distinct morphology. The globules were smaller in the BC samples which contained lower amounts of GlcNAc, such as M1010-1010A and M0416-0416A (Figure 13).

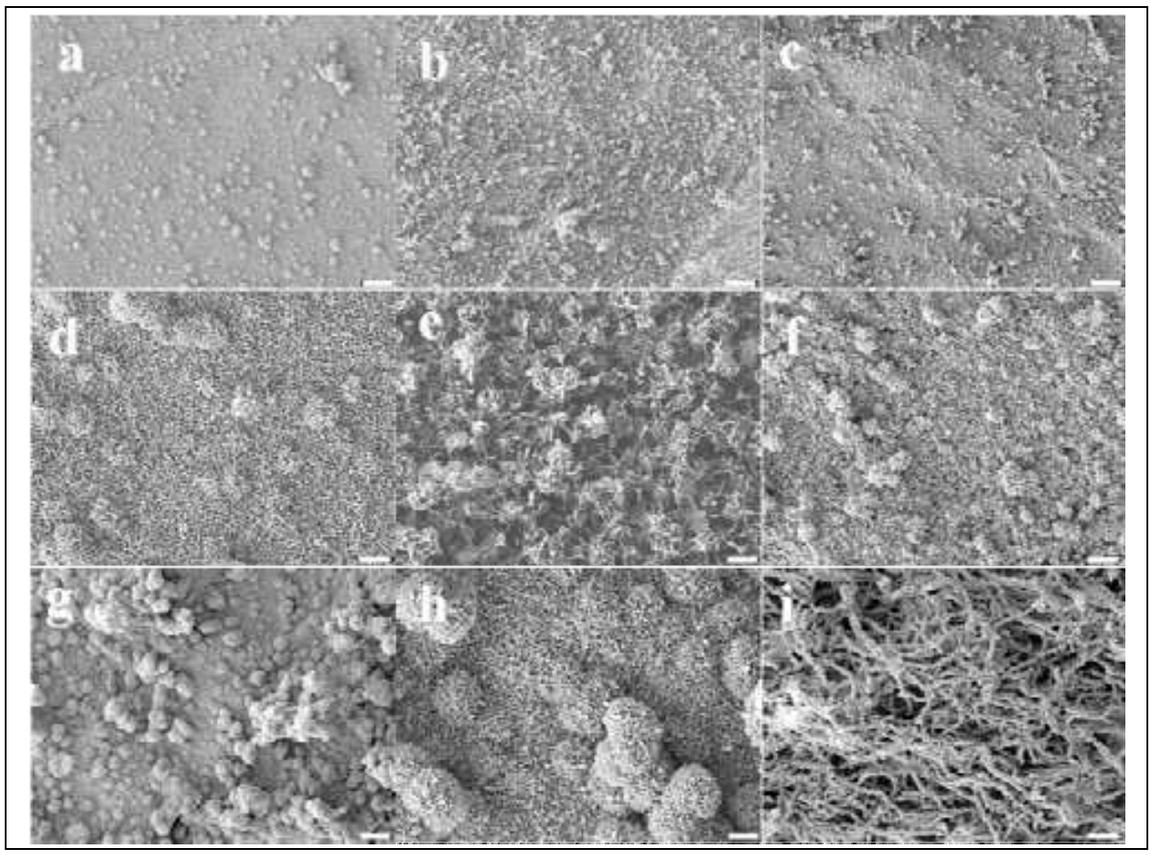


Fig. 13. FE-SEM images of apatite-deposited BC-GlcNAc surfaces after 5 cycles of alternate soaking in calcium and phosphate solutions.
(a,d) M1604-1604A, (b,e) M1010-1010A, (c,f) M0416-0416A, (g,h) surface layer of M0020-1010B, (i) lower layer of M0020-1010B.
d,e,f , and h are high magnification of a,b,c, and g, respectively.
Scale bars: 10 μm for a-c, g, i and 2 μm for d-f, h.

The type of starter culture used for inoculation also affects the formation of apatite. Comparison of Figures 13 b and g (low magnification) or Figures 13 e and h (high magnification) reveals a significant difference in globule size for the BC-GlcNAc 1010 samples. The BC-GlcNAc-M1010-1010A sample in Figures 13 b and e corresponds to an inoculum from starter culture M1010 (Glucose : GlcNAc 10 :10), while the BC-GlcNAc-M0020-1010B sample in Figures 13 g and h was inoculated with starter culture M0020 containing GlcNAc only. The further growth of apatite crystals in M0020-1010B (Figure 13 g, h) led to the formation of globules of about 1-2 μm, whereas globules are likely to grow further in M1010-1010A under the same conditions of soaking. Although the amounts of incorporated GlcNAc are nearly the same in both samples, the type of starter culture used

for inoculation may affect the microfibril network structure, which in turn governs the mineral nucleation and further crystal growth. Figure 13i shows the typical morphology of apatite formed on the lower side of the BC microfibril surface in all BC-GlcNAc samples. It was clear that the mineral nucleation took place around the surface of each microfibril/bundle of BC-GlcNAc. The apatite-coated microfibril diameter (width) was found to be about 1 µm. Based on the observed lateral dimensions of fibril aggregates or ribbons of about 100-110 nm (Figure 6) and 1 µm in width after 5 cycles (~ 5 h) of apatite coating, the mineral deposition rate can be estimated to be 3 nm per min. This interesting observation indicates that the surface properties of BC can be tailored by modifying the BC during biosynthesis.

The weight of calcium-phosphate mineral deposited as a function of the number of soaking cycles is shown in Figure 14. The highest amounts of deposit were observed in the native-BC, BC-TEMPO and BC-TEMPO-Ca samples throughout the soaking cycles. Compared to the BC-GlcNAc samples, the surface modified BC-TEMPO and BC-TEMPO-Ca were characterized by the highest amount of deposit. The presence of carboxylate groups affects not only the crystal nucleation process but also the amount of mineral deposited.

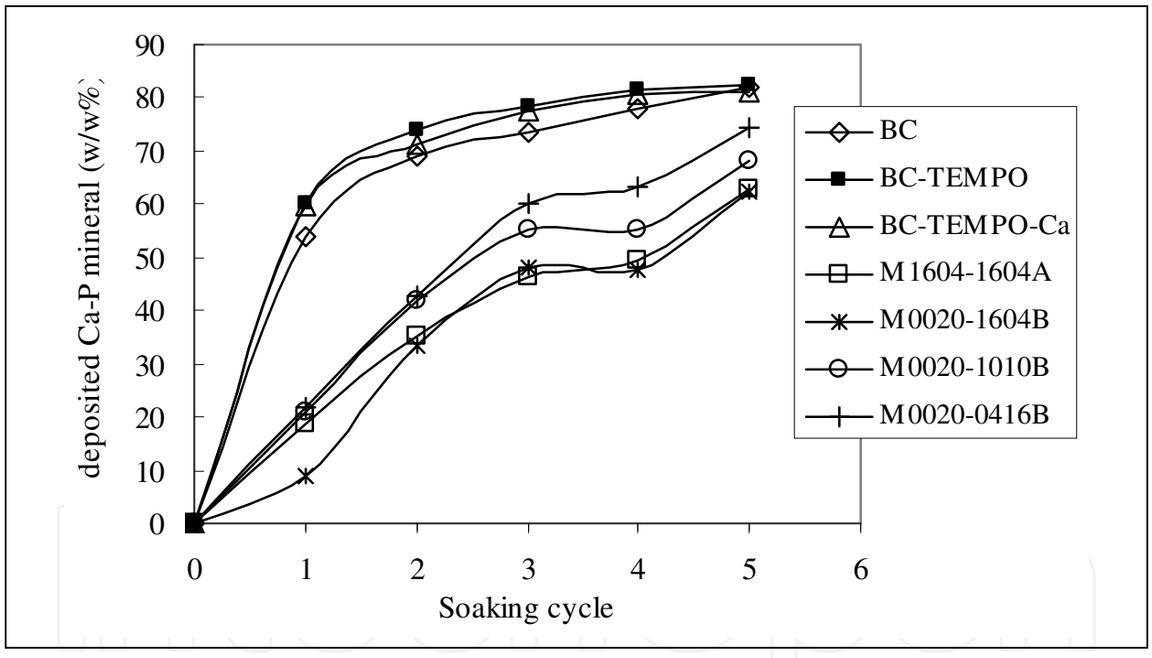


Fig. 14. Relative weight of Ca-P mineral deposit on different BC-GlcNAc as a function of the number of soaking cycles

The BC-GlcNAc samples prepared from the inoculum containing GlcNAc only (M0020) exhibit larger deposits than the samples inoculated with cultures containing various proportions of glucose and GlcNAc. The samples containing lower amounts of incorporated GlcNAc, like M0020-0416B and M0020-1010B, present higher amounts of deposits than M0020-1604B (which exhibits higher incorporated GlcNAc). It can be concluded that the presence of GlcNAc limits the rate of Ca-P nucleation to some extent, although the detailed mechanism remains to be elucidated. The ultrafine network nature of BC (as seen in Figure 8) favours the infiltration of Ca and P ions in the microfibrilar network during the first

soaking cycle and facilitates Ca-P nucleation at the microfibril surface. The presence of incorporated GlcNAc somehow hinders mineral nucleation; as a consequence the overall rate of mineral nucleation on BC microfibril surfaces is slow and the mineral deposit observed at the first soaking cycle is very low. After a gradual increase of the mineral deposition during the first three cycle, the deposition became was fairly stable between the third and fourth cycles in all BC-GlcNAc samples. The entire BC surface was covered by a Ca-P deposit at this stage, which is in agreement with the observation of Ca-P layers in all BC-GlcNAc samples. The increase of Ca-P deposition between the fourth and fifth cycles reflects the further growth of apatite globules visible in FE-SEM images (Figure 13).

The Ca/P molar ratios of all the BC samples analyzed by inductively coupled plasma atomic emission spectroscopy (ICP-AES) are presented in Table 3. Judging from the Ca/P molar ratio, the octacalcium phosphate phase (OCP) is likely to form after the 3rd cycle. Ca/P ratios of all BC samples after the 5th cycle were lower than the theoretical value of hydroxyapatite (1.67). Thus, the Ca-P phase formed on all BC surfaces was a calcium-deficient hydroxyapatite. The BC-GlcNAc samples that were produced from the 0416 medium (Glucose:GlcNAc – 0.4:1.6) inoculated with any type of starter culture (M1604, M0020, M0416) present a Ca/P ratio (1.45-1.51) higher than that of other BC-GlcNAc samples. The highest Ca/P ratio of this sample correlated with its highest deposit weight, as shown in Figure 14.

| | 1st cycle | 3rd cycle | 5th cycle |
|---|---|---|---|
| Native-BC | 1.25 ± 0.002 | 1.29 ± 0.003 | 1.41 ± 0.03 |
| BC-TEMPO | 1.23 ± 0.001 | 1.31 ± 0.002 | 1.46 ± 0.01 |
| BC-TEMPO-Ca | 1.23 ± 0.001 | 1.32 ± 0.003 | 1.39 ± 0.01 |
| | | | |
| *BC-GlcNAc* | | | |
| M1604-1604A | NA | NA | 1.39 ± 0.01 |
| M1604-1010B | NA | NA | 1.46 ± 0.03 |
| M1604-0416B | NA | NA | 1.46 ± 0.01 |
| | | | |
| M0020-1604B | NA | NA | 1.42 ± 0.03 |
| M0020-1010B | NA | NA | 1.41 ± 0.04 |
| M0020-0416B | NA | NA | 1.45 ± 0.07 |
| | | | |
| M1010-1010A | NA | NA | 1.38 ± 0.04 |
| M0416-0416A | NA | NA | 1.51 ± 0.03 |

Table 3. Ca/P molar ratios of different BC samples after 5 cycles of alternate soaking in Ca and P solutions, as measured by ICP-AES

The surface of the BC microfibril network may be considered as a matrix of chemical groups. Therefore, every monomer unit at the surface is a potential site for interaction with calcium and/or phosphate ions. The accessibility of these units at the surface to the ions in 1.5 SBF or calcium and phosphate solutions depends on the orientation of the polymer chains making up the matrix as well as the pore size and pore distribution within the network. Subtle morphological changes at the surfaces of several BC-GlcNAc during apatite formation as well as varying weight deposits and Ca/P ratios are observed accordingly.

## 5. Conclusion

Microbial cellulose has proven to be a remarkably versatile biomaterial and can be used in a wide variety of fields, to produce for instance paper products, electronics, acoustics, and biomedical devices. Various biodegradable and biocompatible polymeric materials have recently been investigated to fabricate inorganic-organic hybrid composites by mimicking the mineralization system of natural bone, with some successful outcomes. However, the search for an ideal biomaterial with properties and functionalities similar to natural bone is a continuing process because no single material can satisfy all the requirements for creating optimal scaffolding properties, such as strength, toughness, osteoconductivity, osteoinductivity, controlled degradation, inflammatory response, and deformability. In this study, the ultrafine 3-D BC network structure with its native unique properties is exploited for the synthesis of materials analogous to natural bone. Our study showed that the formation of apatite is dependent on the presence and type of surface functional groups in the microfibrillar BC network.

Degradation of BC has not been fully evaluated in in vitro and in vivo settings. Other cellulose-based materials have however shown limited degradation. Although the complete degradability of materials for tissue engineering applications is very attractive, it is difficult to practically optimize and synchronize the degradation time and mechanical properties of the materials. Modification of BC by incorporation of lysozyme (an enzyme with anti-bacterial action that is found in body fluids, saliva, sweat and tears) susceptible sugars such as analogues of N-acetylglucosamine (GlcNAc) was performed during microbial synthesis. In addition, GlcNAc shares the structure of some repeated disaccharide units of glycosaminoglycans, which are essential components of extracellular matrices. It is expected that the incorporation of GlcNAc will make BC more degradable and more relevant for end use, for instance in the biomedical area. Subtle changes were observed in the formation of apatite deposits on various BC-GlcNAc surfaces. However, the GlcNAc content of the BC-GlcNAc produced was low (0.36 mole%) compared to other studies (4-18 mole%). The bacterial strain used in our study is different from those reported by others. It is possible that the type of cellulose producing strain influences the incorporation of GlcNAc in BC. This observation suggests that it is worth pursuing this type of investigations to tailor the surface properties of BC to meet the main criteria of mineralized collagen composites such as natural bone and teeth. Such investigations should be complemented by in vitro and in vivo degradation studies.

Since BC is an environmentally friendly biopolymer, its use for materials fabrication for a broad range of applications can be envisaged as an alternative to forest resources. A limitation however is the large-scale production of BC-based composites.

## 6. Acknowledgments

This research was supported by the Japan Society for the Promotion of Science (JSPS) (Grant-in-Aid for Scientific Research number 16004160) and the RISH-Mission project (2006-2007 fiscal year), the Center for Exploratory Research on Humanosphere and the Research Institute for Sustainable Humanosphere at Kyoto University. Prof. Yamanaka from Shinshu University is thanked for the generous gift of the *Acetobacter* strain used in this study. TTN thanks Prof. Isogai and Dr. Saito (University of Tokyo) for their guidance to conduct conductimetric titration, and Dr. Hattori from RISH (Kyoto University) for his guidance to conduct the radio-labelling experiments.

## 7. References


Bäckdahl, H. ; Helenius, G. ; Bodin, A. ; Nannmark, U. ; Johansson, B.R. ; Risberg, B. ; Gatenholm, P. (2006). Mechanical properties of bacterial cellulose and interactions with smooth muscle cells. *Biomaterials*, 27 :2141-2149.

Bigi, A. ; Boanini, E. ; Panzavolta, S. ; Roveri, N. ; Rubini, K. (2002). Bonelike apatite growth on hydroxyapatite-gelatin sponges from simulated body fluid. *J Biomed. Mater. Res.*, 59 : 709-714.

Czaja, W. ; Krystynowicz, A. ; Bielecki, S. ; Brown, R.M. Jr. (2006). Microbial cellulose- The natural power to heal wounds. *Biomaterials*, 27 : 145-151.

de Groot, K. (1983). Bioceramics of calcium phosphate, In : Ceramic of calcium phosphate : Preparation and properties, de Groot, K., (Ed.), 100-114, CRC, Boca Raton, FL.

Di Martino, A. ; Sittinger, M. ; Risbud, M.V. (2005). Chitosan : a versatile polymer for orthopaedic tissue-engineering (review). *Biomaterials*, 26 : 5983-5990.

Elliot, J.C.; Holcomb, D.W.; Young, R.A. (1985) Infrared determination of the degree of substitution of hydroxyl by carbonate ions in human dental enamel. *Calcif. Tissue Int.*, 37: 372-375.

Gilmcher, M.J. (1998). The nature of the mineral phase in bone : biological and clinical applicaitons, In : *Metabolic bone disease and related disorders*, Avioli, L.V. ; Krane, S.M., (Ed.), 23-50, Academic Press.

Helenius, G. ; Bäckdahl, H. ; Bodin, A. ; Nannmark, U. ; Gatenholm, P. ; Risberg, B. (2006). In vivo biocompatibility of bacterial cellulose. *J Biomed. Mater. Res.*, 76A : 431-438.

Hestrin, S. & Schramm, M. (1954). Synthesis of cellulose by *Acetobacter xylinum*, Part 2 : Preparation of freeze dried cells capable of polymerizing glucose to cellulose. *Biochem J.*, 58 : 345-352.

Kim, H.M.; Rey, C.; Glimcher, M.J. (1996) X-ray diffraction, electron microscopy, and Fourier transform infrared spectroscopy of apatite crystal isolated from chicken and bovine calcified cartilage. *Calcif. Tissue Int.*, 59: 58-63.

Klemm, D.; Schumann, D.; Udhardt, U.; Marsch, S. (2001). Bacterial synthesized cellulose-artificial blood vessels for microsurgery. *Prog. Polym. Sci.*, 26: 1561-1603.

Kokubo, T. ; Kushitani, H. ; Sakka, S. ; Kitsugi, T. ; Yamamuro, T. (1990). Solutions able to reproduce in vivo surface-structure changes in bioactive glass-ceramic A-W. *J Biomed. Mater. Res.*, 24 : 721-734.

Koyama, M.; Helbert, W.; Imai, T.; Sugiyam, J.; Henrissat, B. (1997) Parallel –up structure evidences of the molecular directionality during biosynthesis of bacterial cellulose. *Proc. Natl. Acad. Sci. USA.*, 94: 9091-9095.

Lee, J.W. ; Deng, F. ; Yeomans, W.G. ; Allen, A.L. ; Gross, R.A. ; Kaplan, D.L. (2001). Direct incorporation of glucosamine and *N*-acetylglucosamine into exopolymers by *Gluconacetobacter xylinus* (*Acetobacter xylinum*) ATCC 10245 : Production of chitosan-cellulose and chitin-cellulose exopolymers. *Appl. Environ. Microbiol.*, 67(9) : 3970-3975.

Maeda, H. ; Kasuga, T. ; Nogami, M. (2002). Biomimetic apatite formation on poly(lactic acid) composites containing calcium carbonates. *J Mater. Res.*, 17 : 727-730.

Montanari, S. ; Roumani, M. ; Heux, L. ; Vignon, M.R. (2005) Topochemistry of carboxylated cellulose nanocrystals resulting from TEMPO-mediated oxidation. *Macromolecules*, 38 : 1665-1671.

Murugan, R. ; Ramakrishna, S. (2004). Bioresorbable composite bone paste using polysaccharide based nano hydroxyapatite. *Biomaterials*, 25(17) : 3829-3835.

Nge, T.T. & Sugiyama, J. (2007). Surface functional groups dependent apatite formation on bacterial cellulose microfibrils network in a simulated body fluid. *J Biomed. Mater. Res.*, 81A : 124-134.

Nge, T.T. ; Nogi, M. ; Yano, H. ; Sugiyama, J. (2010). Microstructure and mechanical properties of bacterial cellulose/chitosan porous scaffold. *Cellulose*, 17: 349-363.

Ogawa, R. & Tokura, S. (1992). Preparation of bacterial cellulose containing *N*-acetylglucosamine residues. *Carbohydr. Polym.*, 19 : 171-178.

Rey, C.; Collins, B.; Goehl, T.; Dickson, I.R.; Glimcher, M.J. (1989) The carbonate environment in bone mineral: A resolution-enhanced fourier transform infrared spectroscopy study. *Calcif. Tissue Int.*, 45: 157-164.

Rey, C.; Renugopalakrishnan, V.; Shimizu, M.; Collin, B.; Glimcher, M.J. (1991) A resolution-enhanced Fourier transform infrared spectroscopic study of the environment of the $CO_3^{2-}$ ion in the mineral phase of enamel during its formation and maturation. *Calcif. Tissue Int.*, 49: 259-268. (a)

Rey, C.; Shimizu, M.; Collins, B.; Glimcher, M.J. (1991). Resolution-enhanced Fourier-transform infrared spectroscopy study of the environment of phosphate ion in the early deposits of a solid phase of calcium phosphate in bone and enamel and their evolution with age, Part 2: Investigations in $\upsilon_3$ $PO_4$ domain. *Calcif. Tissue Int.*, 49: 383-388. (b)

Saito, T. & Isogai, A. (2004). TEMPO-mediated oxidation of native cellulose : The effect of oxidation conditions on chemical and crystal structures of the water-insoluble fractions. *Biomacromolecules*, 5 : 1983-1989.

Saito, T. & Isogai, A. (2005). Ion-exchange behavior of carboxylate groups in fibrous cellulose oxidized by TEMPO-mediated system. *Carbohydr. Polym.*, 61 : 183-190.

Sato, K.; Kogure, T.; Kumagai, Y.; Tanaka, J. (2001). Crystal orientation of hydroxyapatite induced by ordered carboxyl groups. *J Colloid Interface Sci.*, 240: 133-138.

Schramm, M. & Hestrin, H. (1954). Factors affecting production of cellulose at the air/liquid interface of a culture of Acetobacter xylinum. *J Gen. Microbiol.*, 11: 123-129.

Shirai, A. ; Takahashi , M. ; Kaneko, H. ; Nishimura, S.I. ; Ogawa, M. ; Nishi, N. ; Tokura, S. (1994). Biosynthesis of a novel polysaccharide by *Acetobacter xylinum*. *Int. J Biol. Macromol.*, 16(6) : 297-300.

Suh, J.F.K. & Matthew, H.W.T. (2000). Application of chitosan-based polysaccharide biomaterials in cartilage tissue engineering : review. *Biomaterials*, 21 : 2589-2598.

Svensson, A. ; Nicklasson, E. ; Harrah, T. ; Panilaitis, B. ; Kaplan, D.L. ; Brittberg, M. ; Gatenholm, P. (2005). Bacterial cellulose as potential scaffold for tissue engineering of cartilage. *Biomaterials*, 26 : 419-431.

Takeuchi, A. ; Ohtsuki, C. ; Miyazaki, T. ; Tanaka, H. ; Yamazaki, M. ; Tanihara, M. (2003). Deposition of bone-like apatite on silk fiber in a solution that mimics extracellular fluid. *J Biomed. Mater. Res.*, 65A :283-289.

Uchida, M.; Kim, H.M.; Kokubo, T.; Fujibayashi, S.; Nakamura, T. (2003). Structural dependence of apatite formation on titania gels in a simulated body fluid. *J Biomed. Mater. Res.*, 64A: 164-170.

Uhlin, K.I.; Atalla, R.H.; Thompson, N.S. (1995). Influence of hemicelluloses on the aggregation patterns of bacterial cellulose. *Cellulose*, 2:129-144.

Yokogawa, Y. ; Pazreyes, J. ; Mucalo, M.R. ; Toriyama, M. ; Kawamoto, Y. ; Suzuki, T. ; Nishizawa, K. ; Nagata, F. ; Kamayama, T. (1997). Growth of calcium phosphate on phosphorylated chitin fibers. *J Mater. Sci. Mater. Med.*, 8(7): 407-412.

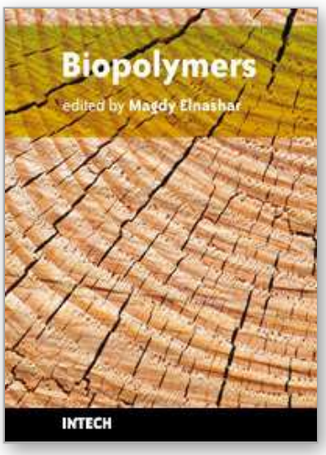


**Biopolymers**

Edited by Magdy Elnashar

ISBN 978-953-307-109-1

Hard cover, 612 pages

**Publisher** Sciyo

**Published online** 28, September, 2010

**Published in print edition** September, 2010

Biopolymers are polymers produced by living organisms. Cellulose, starch, chitin, proteins, peptides, DNA and RNA are all examples of biopolymers. This book comprehensively reviews and compiles information on biopolymers in 30 chapters. The book covers occurrence, synthesis, isolation and production, properties and applications, modification, and the relevant analysis methods to reveal the structures and properties of some biopolymers. This book will hopefully be of help to many scientists, physicians, pharmacists, engineers and other experts in a variety of disciplines, both academic and industrial. It may not only support research and development, but be suitable for teaching as well.



**InTech Europe**

University Campus STeP Ri
Slavka Krautzeka 83/A
51000 Rijeka, Croatia
Phone: +385 (51) 770 447
Fax: +385 (51) 686 166
www.intechopen.com

**InTech China**

Unit 405, Office Block, Hotel Equatorial Shanghai
No.65, Yan An Road (West), Shanghai, 200040, China
中国上海市延安西路65号上海国际贵都大饭店办公楼405单元
Phone: +86-21-62489820
Fax: +86-21-62489821

IntechOpen